

Single and double Auger decay of 4f-ionized mercury including cascade and direct processes

Yu-Long Ma(马玉龙), Fu-Yang Zhou(周福阳), Zhen-Qi Liu(刘振旗), Yi-Zhi Qu(屈一至)
Citation: Chin. Phys. B . 2018, 27(6): 063201. **doi:** 10.1088/1674-1056/27/6/063201

Journal homepage: http://cpb.iphy.ac.cn; http://iopscience.iop.org/cpb

What follows is a list of articles you may be interested in

Branching ratio and angular distribution of ejected electrons from Eu $4f^7 6p_{1/2} nd$ auto-ionizing states

Xiao-Rui Wu(武晓瑞), Li Shen(沈礼), Kai Zhang(张开), Chang-Jian Dai(戴长建), Yu-Na Yang(杨玉娜)
Chin. Phys. B . 2016, 25(9): 093203. **doi:** 10.1088/1674-1056/25/9/093203

Influences of surface and flexoelectric polarization on the effective anchoring energy in nematic liquid crystal

Guan Rong-Hua, Ye Wen-Jiang, Xing Hong-Yu
Chin. Phys. B . 2015, 24(10): 106102. **doi:** 10.1088/1674-1056/24/10/106102

The VMI study on angular distribution of ejected electrons from Eu $4f^7 6p_{1/2} 6d$ autoionizing states

Zhang Kai, Shen Li, Dong Cheng, Dai Chang-Jian
Chin. Phys. B . 2015, 24(10): 103204. **doi:** 10.1088/1674-1056/24/10/103204

Branching ratios of autoionization from Eu $4f^7 6p_{1/2} 6d\ [J]$ autoionizing states

Yan Jun-Gang, Shen Li, Liang Hong-Rui, Dai Chang-Jian
Chin. Phys. B . 2015, 24(8): 083203. **doi:** 10.1088/1674-1056/24/8/083203

Single and double Auger decay of 4f-ionized mercury including cascade and direct processes*

Yu-Long Ma(马玉龙)[1], Fu-Yang Zhou(周福阳)[2], Zhen-Qi Liu(刘振旗)[1], and Yi-Zhi Qu(屈一至)[1,†]

[1] College of Material Sciences and Optoelectronic Technology, University of Chinese Academy of Sciences, Beijing 100049, China
[2] Data Center for High Energy Density Physics, Institute of Applied Physics and Computational Mathematics, Beijing 100088, China

(Received 5 March 2018; revised manuscript received 3 April 2018; published online 30 May 2018)

Single (SA) and double (DA) Auger decay including cascade and direct processes are investigated for Hg $4f^{-1}$ with multiconfiguration Dirac–Fock method and two-step approaches, i.e., knockout and shakeoff mechanisms. Due to the computational effort, only the major transitions are considered to describe the SA and DA decays for the Hg^{+} ions with complex electronic configurations. In order to estimate the Auger transition energies and amplitudes, the reference configuration sets producing the configuration state functions are carefully chosen for balancing electron correlations among the successive singly, doubly and triply ionized mercury. The Auger rates and electron spectra, DA probabilities as well as the populations of the final Hg^{3+} states are obtained. Our results well explain the recent experimental data about the 4f hole states of Hg [Palaudoux J *et al.*, *Phys. Rev.* A **91** 012513 (2015)], and could provide guidance for further studies on complex atoms. Particularly for the DA decay, the contributions of the direct processes, which are neglected in their calculations, are found to be important, accounting for as high as about 38% and 34% of the total DA decays for the $4f^{-1}_{7/2}$ and $4f^{-1}_{5/2}$, respectively.

Keywords: single Auger, cascade double Auger, direct double Auger, Hg $4f^{-1}$

PACS: 32.80.Hd, 32.80.Zb, 31.15.vj **DOI:** 10.1088/1674-1056/27/6/063201

1. Introduction

A hole state of atom is created when a core electron is ionized to continuum orbit by photon, electron, or ion impact. This vacancy could be filled by one outer-shell electron during which it emits an Auger electron, i.e., single Auger (SA) decay, or two Auger electrons, i.e., double Auger (DA) decay. The Auger decay is a nonradiative process that results from Coulomb interaction between electrons. Therefore, the Auger spectroscopy is a powerful tool for investigating electron correlation effects and many-body problems in atomic processes.[1–3] Besides, the Auger spectrum also offers valuable information about the electronic structures of atoms and molecules as the transition energy of the Auger decay depends only on initial core-hole state and final state.[4]

Carlson and Krause[5] first reported the experimental evidence of DA decay by detecting the yields of Ne^{3+} formed by Ne $1s^{-1}$ decay, which has been studied extensively by experimental and theoretical studies over the past several decades[2,3,6–20] since it is essentially responsible for the total Auger intensity. The DA decay could occur by a cascade process where two electrons are emitted stepwise through the creation and decay of an intermediate autoionizing state.[8,9] Apart from the cascade DA, the significant contributions of a direct DA that emits two electrons simultaneously sharing the transition energy, have been demonstrated by experimental studies.[2,12–15] For example, Viefhaus *et al.*[2] demonstrated the existence of the direct process and revealed that it is dominant for the DA decay of Ar $2p^{-1}$, by angle-resolved electron–electron coincidence spectroscopy. Hikosaka *et al.*[12] reported the experimental spectra displaying the Ar^{2+} states populated via direct DA decay following the resonantly excited 2p in Ar. The relative direct and cascade DA probabilities of Ne $1s^{-1}$ are found to be 3.2% and 2.8%, respectively, which indicates that the contributions of the direct and cascade processes are comparable.[14] Recently, even the direct triple Auger decay was observed,[16] and were investigated theoretically in our previous work[17] by using the shakeoff (SO) and knockout (KO) mechanisms.[21] Therefore, in many cases both the cascade and direct processes should be considered for the DA decays.

Mercury is a heavy element with complex electronic configuration (ground configuration $[Kr]4d^{10}5s^{2}4f^{14}5p^{6}5d^{10}6s^{2}$ and [Kr] represents the ground configuration with 36 electrons in neutral Kr), the core–hole states studied experimentally by using a multielectron coincidence detection technique, have received much attention.[18,22–26] For example, Andersson *et al.*[22] reported the experimental SA and DA spectra for the metal Hg with a 4d hole and analyzed the cascade DA decays by the multiconfiguration Dirac–Fock (MCDF) method. Palaudoux *et al.*[18] obtained the DA probabilities and the pop-

*Project supported by the National Key Research and Development Program of China (Grant No. 2017YFA0402300), the National Natural Science Foundation of China (Grant Nos. 11774344 and 11474033), and the Joint Foundation of the National Natural Science Foundation and the China Academy of Engineering Physics (Grant No. U1330117).

†Corresponding author. E-mail: yzqu@ucas.ac.cn

© 2018 Chinese Physical Society and IOP Publishing Ltd

ulations of Hg^{3+} states produced by DA decays of the $4f^{-1}$ and $5p^{-1}$ hole. They also made the calculations to explain the experimental results, but could not produce the reasonable DA probabilities and population of final Hg^{3+} states. A possible reason for this might be that the direct processes were not taken into account in their calculations.

In this work, the theoretical investigations are presented for elucidating the SA and DA decays following the 4f inner-shell ionization of Hg. The direct processes are considered for the DA decay by using two-step approaches, i.e., KO and SO within the framework of the perturbation theory.[21] Besides, the MCDF method[27] is utilized to evaluate the SA transition energy and amplitude. In the practical calculations, the reference configuration sets producing the configuration state functions (CSFs) are chosen for balancing electron correlations since three different successive near-neutral Hg ions, i.e., Hg^{+}, Hg^{2+}, and Hg^{3+} are involved. Finally, our results show good agreement with experimental results[18] about the DA probabilities and populations of final Hg^{3+} states.

2. Theory

The bound-state wave functions with parity P and total angular momentum J for the various Hg ions involved in the Auger decay, are constructed by a CI-type function that is approximated by a linear expansion of CSFs with the same symmetry,

$$\Psi(\gamma,P,J)=\sum_{i=1}^{n}c_i\Phi(\gamma_i,P,J), \tag{1}$$

where γ represents any quantum number required to specify the state with same J, n is the number of CSFs, and c_i denotes mixing coefficient. Generally, the CSF $\Phi(\gamma_i,P,J)$ is an anti-symmetrized linear combination of the products of relativistic one-electron orbitals that are optimized by GRASP2K program,[28] based on the MCDF method. The atomic state function (ASF) is obtained by diagonalizing the Dirac–Coulomb–Breit Hamiltonian matrix to add a high-order relativistic effects such as Breit interaction and QED effects on the basis of CSF.

The SA decay rate can be obtained from[29]

$$A^{1}_{\alpha\beta}=\left|\left\langle\psi^{+}_{\beta},\kappa;J_{\mathrm{T}}M_{\mathrm{T}}\right|\sum_{i<j}^{N}\frac{1}{r_{ij}}\left|\psi_{\alpha}\right\rangle\right|^{2}, \tag{2}$$

where $|\psi_\alpha\rangle$ represents the initial autoionizing state and $|\psi^{+}_{\beta},\kappa;J_{\mathrm{T}}M_{\mathrm{T}}\rangle$ is the final ionic state $|\psi^{+}_{\beta}\rangle$ plus a continuum Auger electron with the relativistic angular quantum number κ. The J_{T} and M_{T} are the total angular momentum and magnetic quantum number of the final state, respectively. In order to obtain the SA rates, the AUGER component of the RATIP program[29] was performed in which the continuum orbitals for the Auger electrons are generated as distorted waves in the potential of final ionic states (please refer to Ref. [30] for details).

In the cascade process, initial autoionizing state primarily decays to intermediate state that is embed energetically in continuum of the next-higher-charge state of ion and will decay further. The cascade DA rate can be obtained from the following expression:

$$A^{2}_{\mathrm{CS}}=\sum_{\beta}A^{1}_{\alpha\beta}A^{1}_{\beta\gamma}\Gamma^{-1}_{\beta}, \tag{3}$$

where $A^{1}_{\beta\gamma}$ is the SA rate from the intermediate state β to the final state γ and Γ_β is the total width of the intermediate state β.

Direct DA is one of the relaxation processes of atoms with an inner-shell vacancy, during which two of outer-shell electrons are emitted simultaneously when a vacancy is filled by another outer-shell electron. This needs a three-body interaction operator for a transition that three single-electron orbitals are changed between the initial and final states. Therefore, we employ the two-step approximate formulas of KO and SO derived from many-body perturbation theory to calculate the direct DA rates.[21]

As shown in our previous work,[17,31] the KO is combined by a primary SA and an inelastic scattering process, in which the second Auger electron may be knocked out of the intermediate ions, i.e., Hg^{2+} through inelastic scattering by the primary Auger electron with specific energy and angular momentum. The direct DA rate of the KO mechanism can be given by

$$A^{2}_{\mathrm{KO}}=\sum_{\beta}A^{1}_{\alpha\beta}\Omega_{\beta\gamma}(\varepsilon_0), \tag{4}$$

where $A^{1}_{\alpha\beta}$ is the SA rate from the initial state α to the intermediate state β , and $\Omega_{\beta\gamma}(\varepsilon_0)$ is the collision strength of the inelastic scattering by the "intermediate" Auger electron with energy ε_0 from the primary SA process.

The SO mechanism resulting from that the second Auger electron is ejected following a sudden change of atomic potential caused by a rapid ejection of the primary Auger electron. The direct DA rate of the SO mechanism can be expressed by

$$A^{2}_{\mathrm{SO}}=\sum_{\beta}A^{1}_{\alpha\beta}\left|\left\langle\psi^{2+}_{\gamma}\ \kappa;J_{\mathrm{T}}M_{\mathrm{T}}\right|\psi^{+}_{\beta}\right\rangle\Big|^{2}, \tag{5}$$

where the matrix element $\langle\psi^{2+}_{\gamma}\kappa;J_{\mathrm{T}}M_{\mathrm{T}}|\psi^{+}_{\beta}\rangle$ represents the overlap integral between the intermediate state β and final state γ with the second Auger electron. Generally, the contribution of the SO mechanism is far less than that of KO.[11,17,31]

The collision ionization strengths and the overlap integrals between the intermediate and final states are calculated using the flexible atomic code[32] with some modifications,[17] based on Dirac–Fock–Slater approach.

3. Electron correlation effects

Auger decays strictly caused by electron–electron interaction hence the electron correlation plays a crucial role in accurately estimating the rates.[31,33,34] Generally, increasing the configuration space of Eq. (1) is one of the ways to include electron correlation. However, the number of the CSFs increases rapidly for the complex configurations in the singly, doubly and triply ionized Hg ions, which challenges the computational capability. Therefore, the configuration space needs to be elaborately considered.

3.1. Auger energies of $4f^{-1}\rightarrow 5p^5 5d^{10} 6s$ and $5p^5 5d^9 6s^2$

As will be discussed in following sections, the highly excited states,such as $5p^5 5d^{10} 6s$ and $5p^5 5d^9 6s^2$ of Hg^{2+} could be populated in SA decay of $4f^{-1}$ states and will be autoionized further into the Hg^{3+} states, which results in the cascade DA decay. The energy levels of Hg $4f^{-1}$ are located among the levels of the $5p^5 5d^{10} 6s$ and $5p^5 5d^9 6s^2$ in Hg^{2+}, and hence the energy level positions should be determined accurately to figure out the energetically allowed channels for the transitions $4f^{-1} \rightarrow 5p^5 5d^{10} 6s$ and $5p^5 5d^9 6s^2$. Furthermore, the inaccuracy of such small transition energies may reduce the reliability of the calculated Auger rates. One could accurately calculate the energies of states by MCDF method, in which the electron correlation is composed of all CSFs that interact with ASFs. Therefore, generating the CSFs is pivotal for capturing the electron correlation effect efficiently, which are obtained by single and double (SD) substitutions from the reference configuration set to virtual orbitals by using the active space (AS) approach.[35] Furthermore, the appropriate reference configuration set are needed to generate the CSF space for the ions with different ionization degrees on the same footing as the balanced correlation considerations are crucially important. For example, in order to determine the transition energies $4f^{-1} \rightarrow 5p^5 5d^{10} 6s$ and $5p^5 5d^9 6s^2$, we first only consider the lowest levels of the $4f^{-1}$ of Hg^+ and $5p^5 5d^{10} 6s$ of Hg^{2+} and treat corresponding configuration as the reference configuration set. The active orbitals are then optimized by variationally determining the eigenenergy of the reference level (namely, the lowest level) for both ions, which is accomplished separately to take into account the relaxation effect. Finally, the splits of the $4f^{-1}$ as well as $5p^5 5d^{10} 6s$ and $5p^5 5d^9 6s^2$ are obtained by these configurations serving as the reference configuration set. Then the sets of active orbitals are enlarged to generate the CSFs for the MCDF calculations as follows.

(i) The occupied orbitals are optimized as spectroscopic ones in the reference configuration set mentioned above. The 5d and 6s orbitals are treated as valence, and the others are regarded as core orbitals, which are kept frozen in subsequent calculations.

(ii) The virtual orbitals are optimized layer by layer up to 9s, 8p, 7d, and 7f orbitals and the CSFs are obtained by SD substitutions from valence orbitals to the virtual ones. This step accommodates the contributions from only valence correlations, which is referred to as the valence–valence (VV) correlation (for the details of the layer-by-layer calculation and generation of the virtual orbitals, please refer to our previous work.[35]

(iii) The ASFs and the mixing coefficients of Eq. (1) are obtained by performing CI calculations with the CSFs obtained by SD substitutions to the orbital basis from step (ii). When the Hamiltonian matrix is diagonalized in the *JJ*-coupled antisymmetric CSFs in this step, the high-order relativistic effects such as Breit interaction and QED effects, which is important for the heavy element of Hg, are included according to the perturbation theory.

As has been illustrated by Cowan,[36] the difference in energy between two successive ions is normally obtained within a satisfying accuracy, the further correlation corrections from the valence *g* orbitals and core are not included due to the computational capacity, which rapidly increases the number of the CSFs.

3.2. Auger transition amplitudes

The influence of the electron correlation effect on the intensity of the cascade DA decay is significant as demonstrated in our previous study for the Ne $1s^{-1}$.[31] The CI approximations including the electron correlation effect are needed to evaluate the Auger transition amplitudes. However, only the main configurations should be included since the numbers of CSFs and transitions increase rapidly and go beyond the computational capability for such a complex case of Hg ions. According to CI scheme, the interactions of the double excitation of $4f^{13} 5p^6 5d^{10} 6s^2 \leftrightarrow 4f^{13} 5p^6 5d^{10} n'l'nl$ (with odd parity) and $5p^6 5d^8 6s^2 \leftrightarrow 5p^6 5d^8 n'l'nl$ (with even parity) are most crucial for Hg^+ and Hg^{2+} sates, respectively. Therefore, doubly excited states such as $5p^6 5d^8 n'l'nl$ (with even parity) of Hg^{2+} could be populated (i.e., shakeup processes[37]), some of which lie above the ionization threshold of Hg^{3+} and may autoionize further into Hg^{3+} states. As this importance has been illustrated in the Auger cascades of the hole state in Cd atom,[38,39] the shakeup processes are included in this work. Due to the admixture of $6p^2$ and $6s^2$, the states $5p^6(5d6s)^9 6p$ (with odd parity) may also be populated in the SA decay where one 6p electron is emitted, i.e., 6s→6p conjugate shakeup process, which were found to be rather weak to include according to the test calculations, just like the case of the resonantly excited neon.[30]

According to the discussion above, the following configurations are considered for describing the main SA and DA decays, which are $4f^{13} 5p^6 5d^{10} 6s^2$ in Hg^+ ions, and $5p^6 5d^{10}$,

$5p^65d^96s$, $5p^65d^86s^2$, $5p^65d^86p^2$, and $5p^65d^86snl$ (nl = 7s, 6d) with even parity, $5p^55d^{10}6s$ and $5p^55d^96s^2$ in Hg^{2+} ions, and $5p^65d^9$, $5p^65d^86s$, and $5p^65d^76s^2$ in Hg^{3+} ions. A balanced treatment of the electron correlation is also necessary for obtaining the resulting DA rates. According to the parity of the state in each ion, the above-mentioned configurations with the lowest average energy are treated as the reference configuration sets that are $4f^{13}5p^65d^{10}6s^2$ for the Hg^+ ion, $5p^55d^{10}6s$ and $5p^65d^{10}$ for the Hg^{2+} ion, and $5p^65d^9$ for the Hg^{3+} ion. Besides, the CSFs with $J > 4$ are not included due to the negligible contributions. Based on these reference configuration sets, the sets of active orbitals are optimized up to 7s, 6p, 6d orbitals by steps (i)–(iii) described in Subsection 3.1, nevertheless all the active orbitals are optimized spectroscopically instead of virtually.

4. Results and discussion

4.1. Single Auger decay

The primary SA rates for the main configurations are listed in Table 1, which are also crucial for the resulting DA rates described by Eqs. (3)–(5). In contrary to the previous study on the SA decay which included only the bound states $5p^65d^86s^2$ for the $N_{6,7}O_{4,5}O_{4,5}$ transitions,[40,41] both the main bound and aotuionizing states of the Hg^{2+} are included in this work. The main SA decay rates that originate from the configurations $5p^65d^{10}$, $5p^65d^96s$, $5p^65d^86s^2$, $5p^55d^{10}6s$, and $5p^55d^96s^2$ are shown in Table 1, and the calculated Auger energies are consistent with experimental results of Hg $4f^{-1}$ [42] and Hg^{2+}.[26] The SA rates are also shown in Fig. 1, indicated by vertical bars with numbers that correspond to the first column of Table 1. To compare with the measurements,[18] the SA rates are convolved to obtain the Auger electron spectra as shown in Fig. 1, with the Gaussian profiles of 1.0 eV and 0.15 eV full width at half maximum (FWHM) in the energy ranges of 50 eV–80 eV and 0 eV–20 eV, respectively, based on the energy resolving power of the apparatus $\Delta E/E = 1.6\%$ in Ref. [18]. For the experimental results,[18] only the populations of the stable states are measured for the Hg^{2+} ions corresponding to about 50 eV–80 eV Auger electron energies, whereas the aotuionizing states corresponding to about 0 eV–20 eV are missing since these states may be autoionized into Hg^{3+} states. Our results reproduce well the experimental measurements in the energy range of 50 eV–80 eV as indicated in Fig. 1, which originates from the configurations $5p^65d^{10}$, $5p^65d^96s$, and $5p^65d^86s^2$. The transitions $4f^{-1} \rightarrow 5p^65d^86s^2$ accounts for 78% and 75% of the total SA rates for $4f^{-1}_{7/2}$ and $4f^{-1}_{5/2}$, respectively, while the ground states $5p^65d^{10}\ ^1S_0$ are rarely populated. This indicates that the removal of the 5d electrons plays a more important role than outer-shell 6s electrons in the SA decay of the Hg with a 4f hole, which shows the importance of relativistic effects (i.e., spin–orbit interaction) in the heavy elements as demonstrated in recent study in the case of the 4f hole in Pb.[43] For the level-to-level transitions, the strongest transitions originate from the states $5p^65d^86s^2\ ^3F_2$ and $^1D_2$ for the $4f^{-1}_{7/2}$ and $4f^{-1}_{5/2}$, respectively, with the contribution of about 20% to the total SA decay.

Table 1. Values of Auger electron energy E and rate A^1 of main channel for the single Auger of Hg $4f^{-1}$ states.

Line	States of Hg^{2+}		$4f_{7/2}$			$4f_{5/2}$		
			E/eV		$A^1/10^{13}$ s^{-1}	E/eV		$A^1/10^{13}$ s^{-1}
			Expt.[26,42]	Ours		Expt.[26,42]	Ours	
1	$5p^65d^{10}$	$^1S_0$	77.87	76.25	0.01	81.94	80.29	0.01
2	$5p^65d^96s$	$^3D_3$	72.55	71.59	0.33	76.62	75.64	0.04
3		$^3D_2$	72.16	71.17	0.42	76.23	75.22	0.08
4		$^3D_1$	70.63	69.78	0.01	74.70	73.83	0.28
5		$^1D_2$	70.29	69.39	0.22	74.36	73.43	0.52
6	$5p^65d^86s^2$	$^3F_4$	65.73	65.14	5.36	69.80	69.18	0.84
7		$^3F_2$	64.72	63.94	8.16	68.79	67.98	0.07
8		$^3F_3$	63.95	63.43	2.35	68.02	67.48	3.37
9		$^3P_2$	63.12	62.41	3.81	67.19	66.46	4.54
10		$^3P_0$	62.66	62.29	2.63	66.73	66.33	0.14
11		$^3P_1$		61.74	3.22		65.79	4.59
12		$^1G_4$	62.19	61.23	4.72	66.26	65.27	6.24
13		$^1D_2$	61.29	60.65	0.92	65.36	64.69	10.75
14		$^1S_0$	58.16	57.26	1.88	62.23	61.30	6.06
15	$5p^55d^{10}6s$	$^3P_2$		12.66	0.26		16.66	0.06
16		$^1P_1$		12.32	0.66		16.32	0.24
17	$5p^55d^96s^2$	$^3F_4$		7.44	0.24		11.44	0.05
18		$^1D_2$		5.98	0.91		9.98	0.05
19		$^3D_3$		4.22	2.03		8.22	0.84
20		$^3D_2$		2.50	1.56		6.5	2.41
21		$^3P_1$		2.36	2.81		6.36	1.27
22		$^3P_0$		2.02	0.06		6.02	0.79
23		$^1F_3$					4.25	2.64
24		$^3D_1$					3.98	2.94

In the energy range of 0 eV–20 eV (shown in Fig. 1), some of the highly excited states $5p^5 5d^{10} 6s$ and $5p^5 5d^9 6s^2$ in Hg^{2+} are populated which account for about 20% of the total primary SA. The ratios of the SA rates are $(5p^5 5d^9 6s^2):(5p^5 5d^{10} 6s) = 8:1$ and 37:1 for $4f_{7/2}^{-1}$ and $4f_{5/2}^{-1}$, respectively. Besides, although not listed in Table 1, the doubly excited sates $5p^6 5d^8 6snl$ ($nl = 7s$, 6d) and $5p^6 5d^8 6p^2$ are populated due to shakeup processes. The binding energies of these 5p hole states and doubly excited sates may lie above the triple ionization threshold,[44] which may decay to Hg^{3+} via a cascade DA decay which will be discussed in the next subsection.

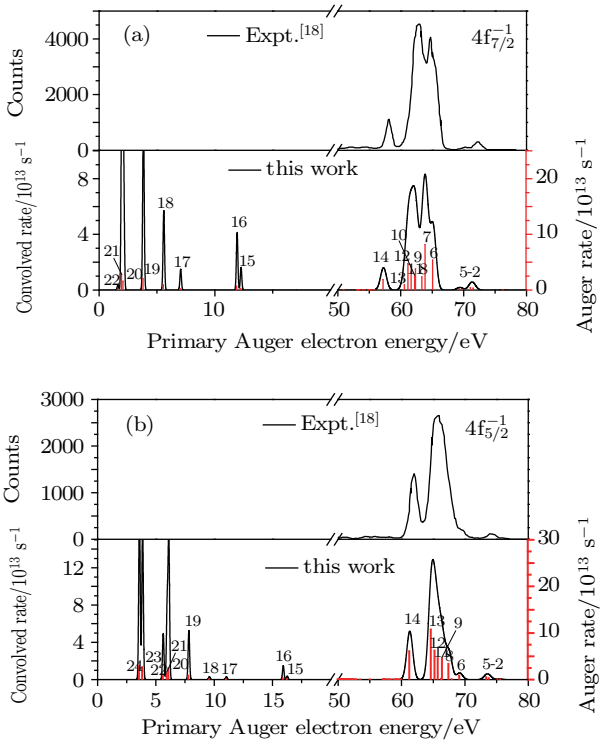


Fig. 1. (color online) Auger electron spectra for single Auger decay of ionized (a) $4f_{7/2}^{-1}$ and (b) $4f_{5/2}^{-1}$ states. Numbered vertical bars indicate Auger rates that corresponds to the first column of Table 1.

4.2. Double Auger decay

Table 2 presents the DA rates (10^{13} s^{-1}) and the relative DA probabilities, which are expressed as the percentages of the specific DA rates in the total decay rate (including SA and DA decays). The calculated total DA probabilities of 30.60% and 32.26% are in good agreement with experimental measurements of 30.5% and 32.0%[18] for the $4f_{7/2}^{-1}$ and $4f_{5/2}^{-1}$, respectively. It is found that the cascade DA processes are dominant with the contributions of about 62% and 66% of the total DA rates for the $4f_{7/2}^{-1}$ and $4f_{5/2}^{-1}$, respectively, which is consistent with the experimental observation.[18] As the dominant processes, the main pathways of the cascade DA are illustrated in Fig. 2 with the intermediate states $5p^5 5d^{10} 6s$, $5p^5 5d^9 6s^2$, $5p^6 5d^8 6snl$ ($nl = 7s$, 6d) and $5p^6 5d^8 6p^2$, where the branching ratio (in percentage) for each pathway is denoted by the number in parenthes. The most prominent pathway is $4f^{-1} \rightarrow 5p^5 5d^9 6s^2 \rightarrow 5d^7 6s^2$ with branching ratios of about 78.0% and 87.8% of the total cascade DA process for the $4f_{7/2}^{-1}$ and $4f_{5/2}^{-1}$, respectively, which leads to the greatest population of the highly excited states $5d^7 6s^2$. This differs from the case of the low- and medium-Z atoms, such as Ne,[14,31] Ar,[11,13] and Kr,[8,9] in which the ground configuration is most preferred. The other two distinct cascade decays are $4f^{-1} \rightarrow 5p^5 5d^{10} 6s \rightarrow 5d^8 6s$ and $4f^{-1} \rightarrow 5p^6 5d^8 6p^2 + 5p^6 5d^8 6snl$ ($nl = 7s$, 6d) $\rightarrow 5d^9$, and their contributions are comparable. In the second step of the cascade DA decays, $5p^5 5d^9 6s^2 \rightarrow 5d^7 6s^2$ and $5p^5 5d^{10} 6s \rightarrow 5d^8 6s$, are fast super Coster–Kronig transitions, which suggests that the short lifetimes for these intermediate states with the lifetime broadenings of about 4 eV–10 eV are an order of magnitude greater than that of initial $4f^{-1}$ state (0.24 eV).[41] Finally, the ratios are determined to be $(5d^7 6s^2):(5d^8 6s):(5d^9) = 12.3 : 2.1 : 1$ and $22.8 : 1.7 : 1$ for the $4f_{7/2}^{-1}$ and $4f_{5/2}^{-1}$, respectively, due to the cascade DA Auger decays.

Table 2. Values of double Auger rate A^2 and DA probability P (in percentage) including the cascade and direct processes to the main configurations of Hg^{3+}.

Hg^+	Hg^{3+}	$A^2/10^{13}$ s^{-1}			P/%			
		Cascade	Direct	DA	Cascade	Direct	DA	Expt.[18]
$4f_{7/2}$	$5d^9$	0.59	0.03	0.62	1.23	0.06	1.29	
	$5d^8 6s$	1.24	3.06	4.30	2.57	6.35	8.92	
	$5d^7 6s^2$	7.28	2.55	9.83	15.10	5.29	20.39	
	total	9.11	5.64	14.75	18.90	11.70	30.60	30.5
$4f_{5/2}$	$5d^9$	0.46	0.02	0.48	0.84	0.04	0.88	
	$5d^8 6s$	0.78	3.04	3.82	1.43	5.54	6.97	
	$5d^7 6s^2$	10.50	2.86	13.36	19.18	5.23	24.41	
	total	11.74	5.92	17.66	21.45	10.81	32.26	32.0

In addition to the cascade processes discussed above, it follows from Table 2 that the direct DA decays account for about 38% and 34% of the total DA decays with rates of 5.64×10^{13} s^{-1} and 5.92×10^{13} s^{-1} for the $4f_{7/2}^{-1}$ and $4f_{5/2}^{-1}$, respectively, which should not be neglected. Neglect of direct processes in their calculation should be the main reason

why they cannot reproduce their measured results.[18] It is found that the direct process almost gives rise to the formations of configurations $5d^86s$ and $5d^76s^2$, while the $5d^9$ are rarely formed. The ratios of direct DA rates are $(5d^86s):(5d^76s^2) = 1.2:1$ and $1.1:1$ for the $4f^{-1}_{7/2}$ and $4f^{-1}_{5/2}$, respectively.

The calculated population of the final states can be directly derived from the Auger rates. To illustrate the contributions from the cascade DA and direct DA processes to the populations of Hg^{3+} states, the DA rates are convolved with Gaussian profile of 0.7-eV FWHM according to the experimental resolution[18] as shown in Fig. 3. In order to compare with experimental results, the experimental binding energies of the ground state of Hg^{3+}[25] are also used. It is found that the calculated populations are in general agreement with experimental results.[18] Besides, figure 3 shows that the contributions from the cascade and direct processes are different for that from the individual configuration. The populations of the $5d^9$ states almost result from cascade DA processes, while the $5d^86s$ states are preferentially populated by direct DA with contribution ratios of the (direct DA): (cascade DA)$= 2.5:1$ and 3.9:1 for the $4f^{-1}_{7/2}$ and $4f^{-1}_{5/2}$, respectively. Meanwhile, the formations of $5d^76s^2$ states are estimated to be (cascade DA):(direct DA)$= 2.9:1$ and $3.7:1$ for the $4f^{-1}_{7/2}$ and $4f^{-1}_{5/2}$, respectively. The discrepancies between the calculated and experimental populations should mainly be caused by the uncertainties of the theoretical energy positions as the state of Hg^{3+} is strongly affected by the electron correlation, particularly for the highly excited states $5d^76s^2$.[25]

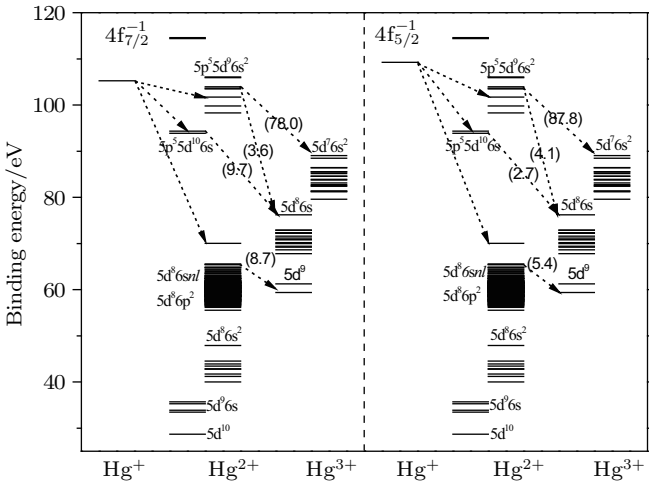


Fig. 2. Illustration of specific pathways for cascade double Auger decays. Arrows indicate possible single Auger transitions, and the branching ratios (in percentage) of each pathway are denoted by the numbers in parentheses.

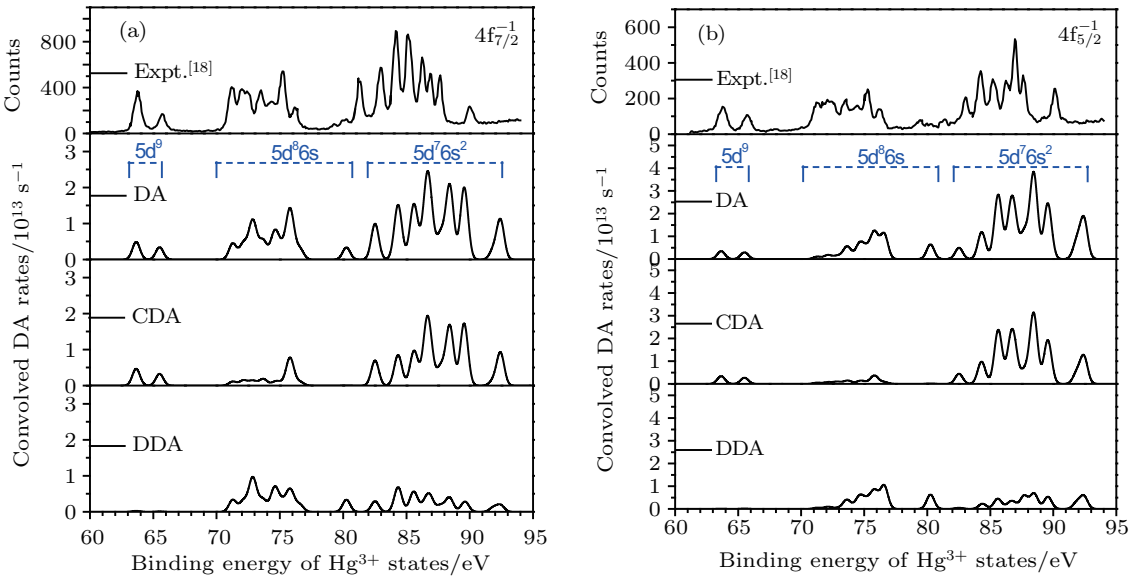


Fig. 3. (color online) Comparisons between the theoretical and experimental populations of the Hg^{3+} after the double Auger decay of ionized (a) $4f^{-1}_{7/2}$ and (b) $4f^{-1}_{5/2}$ states. Values of total population (DA) are obtained by summing the contributions of the cascade (CDA) and direct (DDA) processes. The experimental measurements are obtained by multielectron coincidence spectroscopy.[18]

5. Conclusions

The theoretical investigation of the SA and DA decays including the cascade and direct processes, are presented for the Hg $4f^{-1}$, based on MCDF method. Due to the computational effort, the important configurations are selected for the main Auger channels. The reference configuration sets are chosen to produce the CI space on the same footing for balancing the electron correlations among the successive singly, doubly and triply ionized mercury. The primary SA electron spectra are in good agreement with experimental measurements. The two-step approximate formulas (KO and SO) derived from the perturbation theory are used to simplify the calculation of the direct DA rates. For the cascade DA decays, the transition channels are determined by the large-scale MCDF calculations and the pathways $4f^{-1} \rightarrow 5p^55d^96s^2 \rightarrow 5d^76s^2$ are dominant, leading to the greatest populations of the highly excited states

$5d^7 6s^2$ of Hg^{3+}, which is peculiar to the cases of the low- and medium-Z atoms such as Ne,[14,31] Ar,[11,13] and Kr.[8,9] Our calculated DA probabilities of 30.60% and 32.26% agree with the experimental values of 30.5% and 32.0%[18] for the $4f_{7/2}^{-1}$ and $4f_{5/2}^{-1}$, respectively. Furthermore, our results indicate that the direct processes, which are neglected in the calculations of Ref. [18] , are also important which account for about 38% and 34% of the total DA decays for the $4f_{7/2}^{-1}$ and $4f_{5/2}^{-1}$, respectively.

Acknowledgment

One of the authors, Yizhi Qu, would like to thank professor Yuri Ralchenko for the helpful discussion during his stay in NIST.

References

[1] Stolterfoht N, Havener C C, Phaneuf R A, Swenson J K, Shafroth S M and Meyer F W 1986 *Phys. Rev. Lett.* **57** 74
[2] Viefhaus J, Cvejanović S, Langer B, Lischke T, Prumper G, Rolles D, Golovin A V, Grum-Grzhimailo A N, Kabachnik N M and Becker U 2004 *Phys. Rev. Lett.* **92** 083001
[3] Penent F, Palaudoux J, Lablanquie P, Andric L, Feifel R and Eland J H D 2005 *Phys. Rev. Lett.* **95** 083002
[4] Wang X L, Dong C Z, Xie L Y, Shi Y L, Saber I A and Zhou W D 2012 *Chin. Phys. Lett.* **29** 103201
[5] Carlson T A and Krause M O 1965 *Phys. Rev. Lett.* **14** 390
[6] Kanngießer B, Jainz M, Brünken S, Benten W, Gerth C, Godehusen K, Tiedtke K, van Kampen P, Tutay A, Zimmermann P, Demekhin V F and Kochur A G 2000 *Phys. Rev. A* **62** 014702
[7] Brünken S, Gerth C, Kanngießer B, Luhmann T, Richter M and Zimmermann P 2002 *Phys. Rev. A* **65** 042708
[8] Andersson E, Fritzsche S, Linusson P, Hedin L, Eland J H D, Karlsson L and Feifel R 2010 *Phys. Rev. A* **82** 043418
[9] Palaudoux J, Lablanquie P, Andric L, Ito K, Shigemasa E, Eland J H D, Jonauskas V, Kučas S, Karazija R and Penent F 2010 *Phys. Rev. A* **82** 043419
[10] Suzuki I H, Hikosaka Y, Shigemasa E, Lablanquie P, Penent F, Soejima K, Nakano M, Kouchi N and Ito K 2011 *J. Phys. B: At. Mol. Opt. Phys.* **44** 075003
[11] Zeng J L, Liu P F, Xiang W J and Yuan J M 2013 *Phys. Rev. A* **87** 033419
[12] Hikosaka Y, Lablanquie P, Penent F, Selles P, Kaneyasu T, Shigemasa E, Eland J H D and Ito K 2009 *Phys. Rev. A* **80** 031404(R)
[13] Hikosaka Y, Lablanquie P, Penent F, Selles P, Shigemasa E and Ito K 2014 *Phys. Rev. A* **89** 023410
[14] Hikosaka Y, Kaneyasu T, Lablanquie P, Penent F, Shigemasa E and Ito K 2015 *Phys. Rev. A* **92** 033413
[15] Viefhaus J, Grum-Grzhimailo A N, Kabachnik N M and Becker U 2004 *J. Electron Spectrosc. Relat. Phenom.* **141** 121
[16] Müller A, Borovik A, Jr, Buhr T, Hellhund J, Holste K, Kilcoyne A L D, Klumpp S, Martins M, Ricz S, Viefhaus J and Schippers S 2015 *Phys. Rev. Lett.* **114** 013002
[17] Zhou F Y, Ma Y L and Qu Y Z 2016 *Phys. Rev. A* **93** 060501(R)
[18] Palaudoux J, Huttula S M, Huttula M, Penent F, Andric L and Lablanquie P 2015 *Phys. Rev. A* **91** 012513
[19] Hindi M M, Zhu L, Avci R, Miočinović P M, Kozub R L and Lapeyre G J 1996 *Phys. Rev. A* **53** R3716
[20] Hu H W and Dong C Z 2006 *Acta Phys. Sin.* **55** 6326 (in Chinese)
[21] Amusia M Y, Lee I S and Kilin V A 1992 *Phys. Rev. A* **45** 4576
[22] Andersson J, Beerwerth R, Roos A H, Squibb R J, Singh R, Zagorodskikh S, Talaee O, Koulentianos D, Eland J H D, Fritzsche S and Feifel R 2017 *Phys. Rev. A* **96** 012505
[23] Huttula S M, Soronen J, Huttula M, Penent F, Palaudoux J, Andric L and Lablanquie P 2015 *J. Phys. B: At. Mol. Opt. Phys.* **48** 115001
[24] Huttula M, Huttula S M, Fritzsche S, Lablanquie P, Penent F, Palaudoux J and Andric L 2014 *Phys. Rev. A* **89** 013411
[25] Huttula M, Huttula S M, Lablanquie P, Palaudoux J, Andric L, Eland J H D and Penent F 2011 *Phys. Rev. A* **83** 032510
[26] Eland J H D, Feifel R and Edvardsson D 2004 *J. Phys. Chem. A* **108** 9721
[27] Grant I P 2007 *Relativistic Quantum Theory of Atoms and Molecules* (New York: Springer)
[28] Jönsson P, He X, Froese Fischer C and Grant I P 2007 *Comput. Phys. Commun.* **177** 597
[29] Fritzsche S 2012 *Comput. Phys. Commun.* **183** 1525
[30] Stock S, Beerwerth R and Fritzsche S 2017 *Phys. Rev. A* **95** 053407
[31] Ma Y L, Zhou F Y, Liu L and Qu Y Z 2017 *Phys. Rev. A* **96** 042504
[32] Gu M F 2008 *Can. J. Phys.* **86** 675
[33] Jonauskas V, Kučas S and Karazija R 2011 *Phys. Rev. A* **84** 053415
[34] Huttula S M, Heinäsmäki S, Aksela H, Kukk E, Huttula M and Aksela S 2003 *Phys. Rev. A* **67** 052703
[35] Zhou F Y, Qu Y Z, Li J G and Wang J G 2015 *Phys. Rev. A* **92** 052505
[36] Cowan R D 1981 *The Theory of Atomic Structure and Spectra* (Berkeley: University of California Press)
[37] Ding X B and Dong C Z 2012 *Chin. Phys. Lett.* **29** 063201
[38] Andersson J, Beerwerth R, Linusson P, Eland J H D, Zhaunerchyk V, Fritzsche S and Feifel R 2015 *Phys. Rev. A* **92** 023414
[39] Beerwerth R and Fritzsche S 2017 *Eur. Phys. J. D* **71** 253
[40] Lohmann B 1993 *J. Phys. B: At. Mol. Opt. Phys.* **26** 1623
[41] Aksela H, Aksela S, Jen J S and Thomas T D 1977 *Phys. Rev. A* **15** 985
[42] Svensson S, Mårtensson N, Basilier E, Å P, Gelius U and Siegbahn K 1976 *J. Electron Spectrosc. Relat. Phenom.* **9** 51
[43] Patanen M, Urpelainen S, Kantia T, Heinäsmäki S, Aksela S and Aksela H 2011 *Phys. Rev. A* **83** 053408
[44] Kramida A, Ralchenko Y, Reader J and NIST ASD Team, NIST Atomic Spectra Database (ver. 5.5.1), [online]. Available: https://physics.nist.gov/asd.